Diurnal variation of turbulence characteristics in Lake Garda

W.K. Lenstra[a], L. Hahn-Woernle[a,], E. Matta[b], M. Bresciani[b], C. Giardino[b], N. Salmaso[c], M. Musanti[b], G. Fila[b], R. Uittenbogaard[e], M. Genseberger[e], H. van der Woerd[d], H.A. Dijkstra[a]

[a] *Institute for Marine and Atmospheric research Utrecht, Center for Extreme Matter and Emergent Phenomena, Utrecht University, The Netherlands*
[b] *Italian National Research Council - Institute for the Electromagnetic Sensing of the Environment*
[c] *Sustainable Agro-ecosystems and Bioresources Department, IASMA Research and Innovation Centre, Istituto Agrario de S. Michele all'Adige - Fondazione E. Mach, Via E. Mach1, 38010, S. Michele all'Adige, Trento, Italy*
[d] *Institute for Environmental Studies (IVM), De Boelelaan 1085, 1081 HV Amsterdam, The Netherlands*
[e] *Deltares, P.O. Box 177, 2600 MH, Delft The Netherlands*

Abstract

Turbulent mixing strongly influences the distribution of phytoplankton in holomictic lakes such as Lake Garda. During March 5-7, 2014, high-resolution vertical measurements were made of temperature and fluorescence in the upper 100 meters of Lake Garda, using a free-falling microstructure profiler. Fluorescence profiles are compared with in-situ and satellite measurements provided by MODIS AQUA. From the measured vertical temperature profiles, turbulence characteristics such as the kinetic energy dissipation ε, the thermal variance dissipation χ and the vertical mixing coefficient K_T were determined. These appear to be the first direct measurements of K_T and, although the observation period is short, they show interesting temporal (diurnal) variations in K_T which can be connected to the changes in the surface wind stress and background stratification. Phytoplankton concentrations in the mixed layer are found to decrease with the magnitude of the vertical mixing coefficient.

1. Introduction

In lakes at temperate latitudes the plankton community evolves in an annually recurring pattern [26], with the abrupt onset of phytoplankton growth in spring as a starting point. The timing of the onset of the phytoplankton growth is controlled predominantly by abiotic factors such as vertical mixing and variations in solar radiation [1]. In deep lakes, interannual variations in the timing of these blooms dominantly result from changes in vertical mixing rather than solar variations and temperature [20].

Lake Garda (45 °40' N and 10 °41' E) is a deep lake with relatively low concentration of chlorophyll-a (chl-a) and therefore can be classified as an oligo-mesotrophic basin [5]. With a surface area of 368 km^2 it is the largest fresh water lake in Italy. Lake Garda has a mean depth of 133 m, a maximum depth of 350 m and a total volume of 49 million m^3. The concentration of chl-a in Lake Garda ranges from 0.5 to 12 mg m^{-3} [5].

It was shown that external factors, such as winter air temperature, spring lake temperature and extent of surface nutrient enrichment, had significant effects on the phytoplankton distributions in Lake Garda over the period 1990-2003 [24]. During this period, three complete overturns occurred following harsh winters (1991, 1999 and 2000) associated with increased mixed layers depths. These overturns, by bringing nutrients to surface layers, determined different transient effects on several phytoplankton groups with peaks of different groups at different times within the period from April to August.

Climate change is unequivocally connected to an increase in surface temperature over lakes in Western Europe, such as the relatively large Lake Garda. Increased temperatures will affect upper lake temperatures and thermal stratification and hence are expected to change mixing conditions. Climate warming may therefore induce a shift in the timing and onset of the growth of phytoplankton and hence strongly affect food-web interactions with zooplankton and fish [25]. It is therefore important to understand the detailed causal chain between climate change, changes in vertical mixing and the timing and extent of phytoplankton blooms.

In this paper, we report on first direct measurements of turbulence characteristics at 4 locations in the southern part of Lake Garda using a SCAMP (Self Contained Autonomous Microstructure Profiler) during March 5-7, 2014. From the SCAMP data, profiles of the kinetic energy dissipation ε, the thermal variance dissipation χ and the vertical mixing coefficient K_T were determined. Using the fluorometer of the SCAMP, also the vertical profile of

fluorescence is measured.

Together with data of meteorological forcing (source: MeteoSwiss (high resolution model COSMO-2)F), nutrient concentrations (water samples) and remote sensing data (MODIS AQUA), we aim to make a preliminary assessment of the connection between the diurnal variations of vertical mixing and upper layer chl-a concentrations. In section 2, an overview is provided of the field measurements with the SCAMP, the additional data obtained and the data processing. The main results and analyses are presented in section 3 and a summary and discussion of these results is provided in section 4.

2. Data and Methods

2.1. Field work locations

The measurements in Lake Garda were carried out over the period of three days from March 5-7, 2014. Over this period, measurements were done at 4 different stations. In Fig. 1, a map of the southern part of Lake Garda is shown where the dots represent the locations of the different stations. The number of profiles measured with the SCAMP are dependent of the circumstances of the lake. When a lake is stratified, more measurements are needed to get reliable results than when a lake is homogeneously mixed where vertical profiles are more comparable to each other. Another influence is the weather, during rough weather it is more difficult to obtain good quality measurements than during quiet weather.

In Table 1, the coordinates, maximum measured depth and number of measurements at the different stations are listed. The field trip covered three days of measurements which were split into a morning (before 13:00) and an afternoon (after 13:00) set. Measurements at the red and black station (Fig. 1) were done in the afternoon and at the blue station only in the morning. At the green station three measurement sets were taken, the morning of March 6 and both morning and afternoon of March 7.

2.2. SCAMP measurements

The SCAMP is a free-falling instrument with a fall speed of approximately 0.1 $m\ s^{-1}$ and a temporal resolution of 100 Hz. This results in a measurement approximately every millimeter, which is needed for characterizing the small-scale turbulent motions. The SCAMP measures vertical profiles of temperature, fluorescence and photo-synthetically active radiation

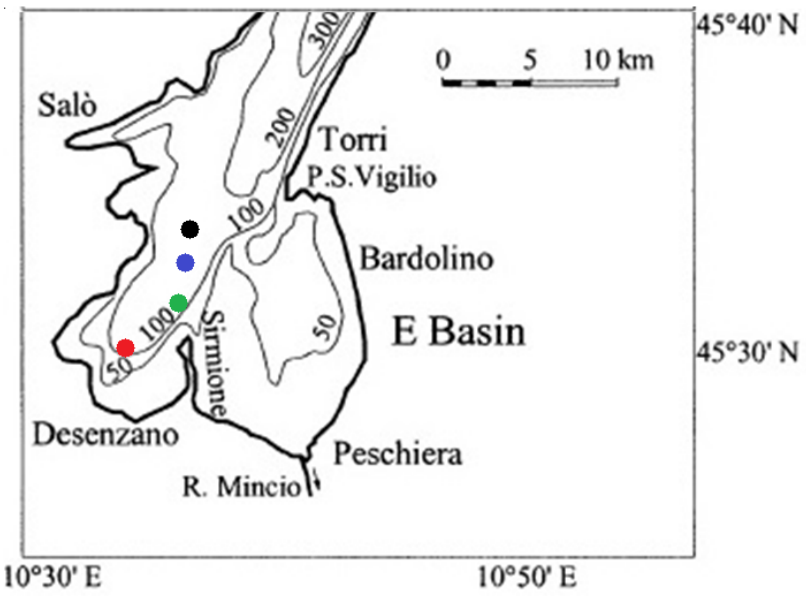

Figure 1: Stations (colored dots) where SCAMP measurements were done during March 5-7 in Lake Garda. The precise locations and details on the number of profiles can be found in Table 1.

Station (Fig. 1)	**Location**	**Max. depth of measurement**	**Number of measurements**	**Date**
Blue	45.544°N, 10.618°E	100 m	6	5 March
Black	45.563°N, 10.621°E	100 m	6	5 March
Red	45.494°N, 10.567°E	45 m	8	6 March
Green	45.524°N, 10.602°E	75 m	5+5+8	6 & 7 March

Table 1: Detailed information about measurement locations in Lake Garda during March 5-7, 2014.

(PAR) of the upper layer in high resolution. The maximum measuring depth of the SCAMP is 100 m which gives a large enough range for measuring turbulence in the upper layer of a lake.

The SCAMP measures the vertical temperature profile with 2 fast response thermistors and 1 accurate thermistor. The fast sensors have a precision of 0.05 °C, the more accurate thermistor measures with a precision of 0.02 °C. The depth is measured with a pressure sensor with a precision of 0.5% [10]. The depth channel is used to calculate the free-fall velocity of the SCAMP. Attached to the top end of the SCAMP there is a PAR sensor. Above the thermistors there is an inlet where water can flow through the SCAMP from which the fluorescence is measured. Precision of the fluorometer and PAR sensor measurements are not prescribed. The measurements of fluorescence are given in volt and have to be calibrated with in-situ or satellite measurements of chl-a, this is further described in Appendix A. Detailed information about the SCAMP can be found at the homepage of PME ($http://www.pme.com/HTML\%20Docs/Scamp\_Home.html$).

The SCAMP is provided with MATLAB software with which the measured profiles are preprocessed before analysis. First, a sharpening, smoothening, trimming and second-order Butterworth Brick-Wall filter are performed as described by Fozdar et al. (1985) [4]. Next, the measured profiles are depth-binned; here one meter bins are chosen because of a trade-off between having sufficient vertical resolution and good statistical robustness. The final temperature profiles consist of one value per bin which is the arithmetic mean of the values in this bin.

2.3. Determination of turbulence quantities

When the assumption is made that dependent quantities are uniform in the horizontal and that the temporal mean vertical velocity is zero ($\overline{w} = 0$) [19], the temperature variance equation can be written as

$$\frac{\partial}{\partial t}\overline{(T')^2} = -2\overline{(w'T')}\frac{\partial \overline{T}}{\partial z} - \chi. \tag{1}$$

Here, the first term on the right hand side is the production of thermal variance by the vertical heat flux. The second term describes the dissipation of thermal variance by thermal diffusion χ ($K^2\ s^{-1}$) and is given by

$$\chi = 6\kappa\overline{(\frac{\partial T'}{\partial z})^2}. \tag{2}$$

where κ ($m^2 s^{-1}$) is the thermal diffusivity. Assuming that production and dissipation terms balance when averaged over time [22], the left hand side of (1) is zero. Using a first order closure for the turbulent heat flux, the vertical mixing coefficient K_T ($m^2 s^{-1}$) is found from

$$\overline{w'T'} = -K_T \frac{\partial \overline{T}}{\partial z} \qquad \rightarrow \qquad K_T = \frac{\chi}{2} \left(\frac{\partial \overline{T}}{\partial z} \right)^{-2}. \tag{3}$$

In the turbulent kinetic energy equation, the relevant quantity is the dissipation of turbulent kinetic energy, indicated here by ε ($m^2 s^{-3}$). To determine ε, processes at the Batchelor length scale are considered, where advection and diffusion of heat approximately balance. The Batchelor length scale (l_B) is given by

$$l_B = \left(\frac{\nu \kappa^2}{\varepsilon} \right)^{\frac{1}{4}} \tag{4}$$

where ν is the kinematic viscosity ($m^2 s^{-1}$). The Batchelor wavenumber is the inverse of the Batchelor length scale ($k_B = 1/l_B$) and can be estimated by fitting a (Batchelor) spectrum to the temperature gradient measurements. We used the maximum likelihood method developed by Ruddick et al. [22], which is further explained in Appendix B. When k_B is determined, ε can be estimated by

$$\varepsilon_{segment} = (2\pi k_{Bsegment})^4 \nu_{segment} \kappa^2 \tag{5}$$

Where $\nu_{segment}$ is the arithmetic mean of the molecular kinematic viscosity in the segment and $k_{Bsegment}$ is the optimal value of the Batchelor wave number (in cpm). Dillon et al. (1980) [3] and Oakley et al. (1982) [17] concluded that ε determined indirectly through Batchelor fitting agrees within a factor 2 with the ε determined using vertical shear velocity fluctuations of the flow .

2.4. Additional data

During the three day campaign, water samples at different depths (surface, 15 m, 30 m and 45 m) were collected for subsequent laboratory analyses to determine chl-a and nutrient concentrations chl-a. The concentration of chl-a was measured according to Lorenzen et al. (1967) [15].

Measurements of surface chl-a concentrations done by MODIS AQUA can be used to calibrate the SCAMP measurements. The way this data is

processed from the satellite measurements is further discussed in Appendix C.

COSMO-2 data, source: MeteoSwiss, is used to evaluate the meteorological circumstances during the field trip, because of its high spatial and temporal resolution (1 hour, 2.2 km) it can solve small variations of meteorological variables over the lake. This data is used to calculate meteorological parameters which are discussed below. The wind stress on the water surface is calculated with help of

$$\tau_0 = \rho_{air} C_D U_{10}^2, \tag{6}$$

where C_D is the wind-drag coefficient ($1.3 * 10^{-3}$) and U_{10} ($m\ s^{-1}$) is the wind speed measured at a height of 10 meters. The net surface buoyancy flux in fresh water is determined from

$$B_t = \frac{g \alpha Q_0}{\rho_s C_{pw}}, \tag{7}$$

where g is the gravitational acceleration (9.81 $m\ s^{-2}$), α (K^{-1}) is the thermal coefficient of expansion, ρ_s ($kg\ m^3$) is the water density at atmospheric pressure, C_{pw} ($J\ kg^{-1}\ K^{-1}$) the specific heat capacity of water and Q_0 ($W\ m^{-2}$) the net surface heat flux.

3. Results

3.1. Meteorological forcing

In Fig. 2 the wind speed measured during the three different days is shown.

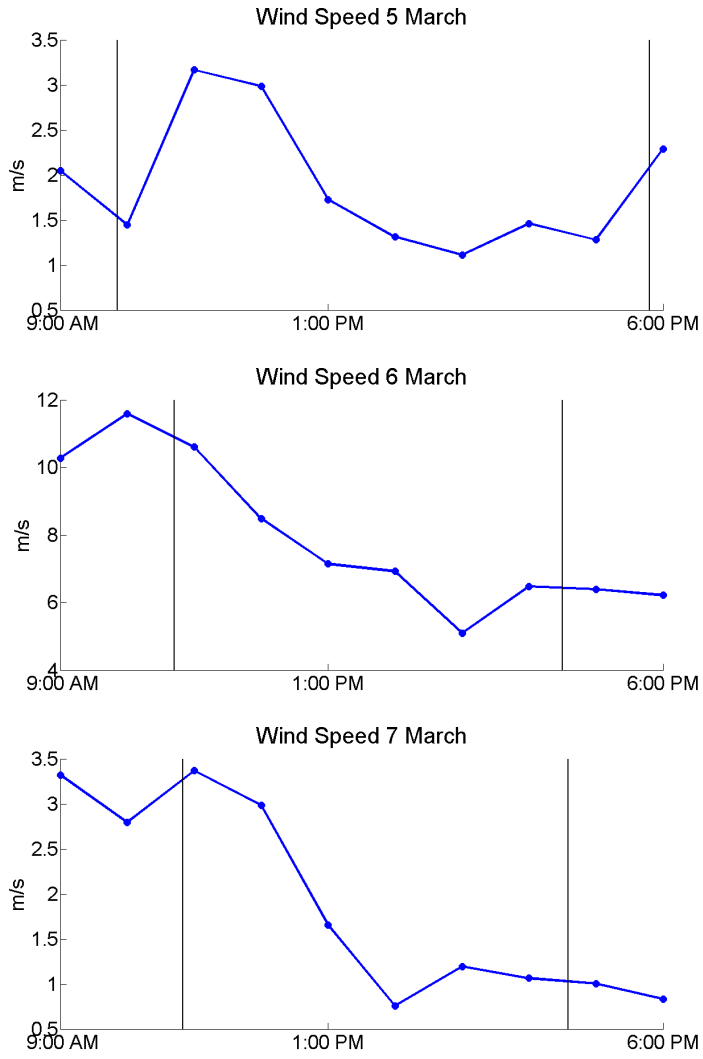

Figure 2: Wind speed (at 10 meter) output of COSMO-2 model run (data obtained from MeteoSwiss) over the 3 measurements days. The average wind speed is taken over the southern part of lake Garda (45.48 - 45.62 °N, 10.57 - 10.66 °W). The area between the vertical black lines indicates the period where measurements were done. Figures are plotted against different y-axis.

During the field trip, diurnal variation in the meteorological circumstances was observed. In the morning relatively high wind speed and high waves occurred while in the afternoon wind speed decreased and waves almost

vanished.

Fig. 3 shows the radiation balance ($W\ m^{-2}$), Buoyancy flux ($W\ kg^{-1}$) and wind stress ($N\ m^{-2}$) during the lake Garda field trip calculated from COSMO-2 meteorological data output. These quantities allow to assess the relation between the atmospheric forcing and the turbulence in the mixed layer (ML). The radiation balance is directed from the lake towards the atmosphere.

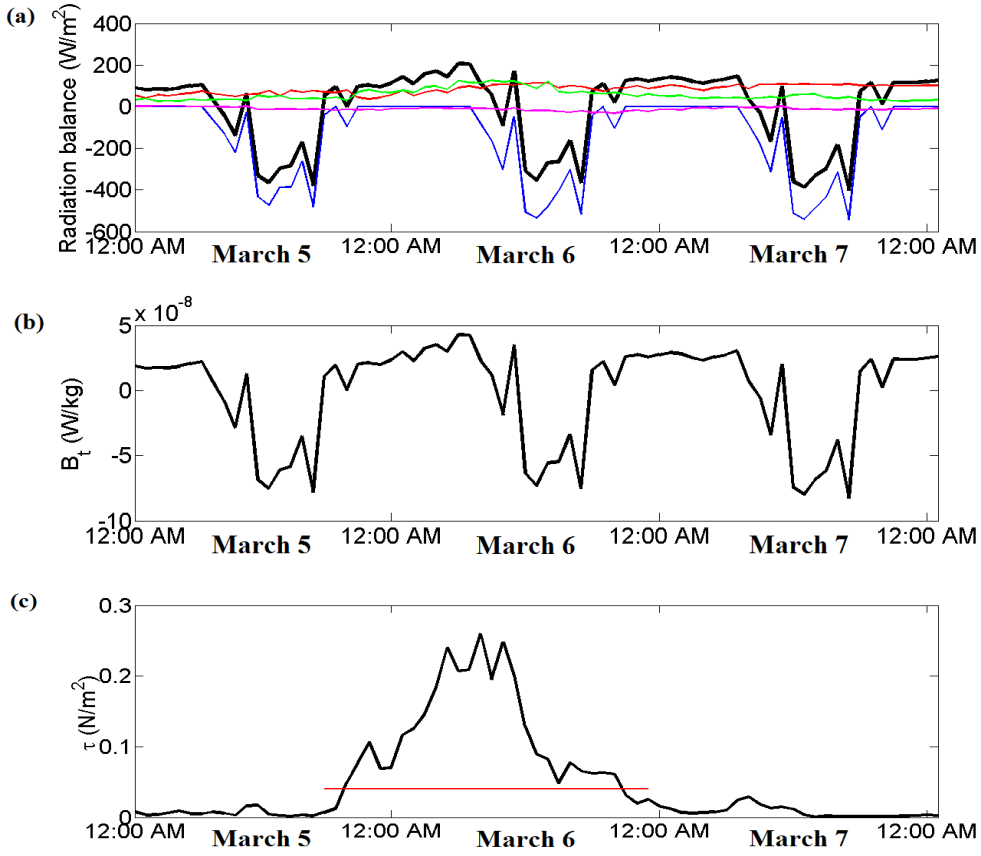

Figure 3: Meteorological circumstances during the lake Garda field trip, output of COSMO-2 (data obtained from MeteoSwiss). COSMO-2 output is averaged over the southern part of lake Garda (45.48 - 45.62 °N, 10.57 - 10.66 °W). **a)** Radiation balance; net surface heat flux (black), net shortwave heat flux (blue), net longwave heat flux (red), sensible heat flux (pink), latent heat flux (green). **b)** Buoyancy flux ($W\ kg^{-1}$) **(c)** Wind stress ($N\ m^{-2}$) red line indicates the critical wind stress level for turbulence avoidance discussed in section 3.4**.**

During the measurement period the net surface heat flux was directed from the atmosphere towards to ocean, the buoyancy flux ranges from -4.3 - 8.3 $\times$ 10^{-8} W kg^{-1}. Stabilizing the upper lake during the day and destabilizing during the night. The surface wind stress ranges from 0.0001 to 0.2598 N m^{-2} with a large peak in wind speed during the night of March 6.

3.2. Observed vertical profiles

In Fig. 4, vertical temperature profiles are plotted. To take the changing meteorological circumstances into account, a distinction is made between measurements in the morning and in the afternoon.

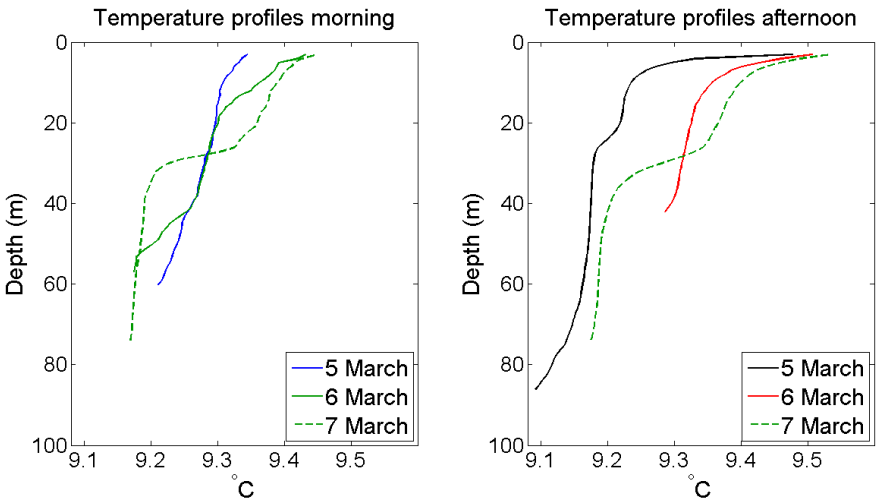

Figure 4: Trimmed-smoothed-sharpened-filtered and binned temperature profiles that are station averaged and divided in a morning and afternoon measurement set. Data is discarded when there are less than three data points for a certain depth. The colors of the lines correspond to the color of the stations as shown in Fig. 1.

During the day the depth binned station averaged temperature profiles show an increase in stratification because of heating from the sun and calmer weather conditions in the afternoon. The measurements done on March 5 show a homogeneously ML with a small sloping profile in the morning, while in the afternoon a small temperature gradient can be seen around the depth of 25 meters. On March 6 and 7, morning and afternoon temperature profiles look similar to each other, but in the afternoon the surface temperature is

increasing. Maximum measurement depth at March 6 is limited because measurements were done at the shallow part of lake Garda.

Over the three days a stratification build up is seen in the temperature profiles measured in the morning with a relatively large temperature gradient appearing near 30 m depth on March 7. The same also holds for the temperature measurement in the afternoon although the temperature gradients are less obvious on March 5 and 6. On March 6, no clear temperature gradient was found because of a limited maximum measuring depth at the measured station.

Fig. 5 presents the vertical profiles of K_T, χ and ε (for all 3 days). Missing data points (white areas) occur due to an insufficient Batchelor fit. The Batchelor fit rejection criteria are discussed in Appendix B. The vertical profiles of the turbulence characteristics show relatively high values in the morning and lower values in the afternoon. This diurnal variation is associated with the changing meteorological forcing, in particular the changes in wind stress.

The K_T values have a maximum around the middle of the ML and decrease towards the top, where the boundary reduces the size of the turbulent eddies, and towards the bottom of the ML, where the stability of the water column reduces turbulent mixing. High values of vertical mixing are found below the ML in the afternoon of March 5 and in the morning of March 7. χ is largely affected by thermal stratification and its largest values are found near the surface. The ε measured on March 6 and 7 have higher values in the morning than in the afternoon. On March 5 there is no large difference between the morning and afternoon measurements.

In Fig. 6 (a-c) all the binned values of the turbulence characteristics K_T , χ and ε measured within the ML are plotted. It is chosen to only plot values measured within the ML because the ML is in direct contact with the atmosphere and this way the effect of changing meteorological forcing on turbulence in the ML can be studied.

The depth of the ML is usually determined by the depth at which the temperature difference with respect to the surface is $0.5°C$ [14]. Yet, in our case of small temperature gradients this definition is not very useful. To take the small temperature gradient into account we defined the mixed layer depth (MLD) as the depth where the temperature deviated $0.11°C$ from the average temperature over the first 10 meters. The averaging over the first 10 meters was done to avoid a strong influence of relatively high temperatures at the surface (Fig. 4). The value of $0.11°C$ was chosen out of experience and

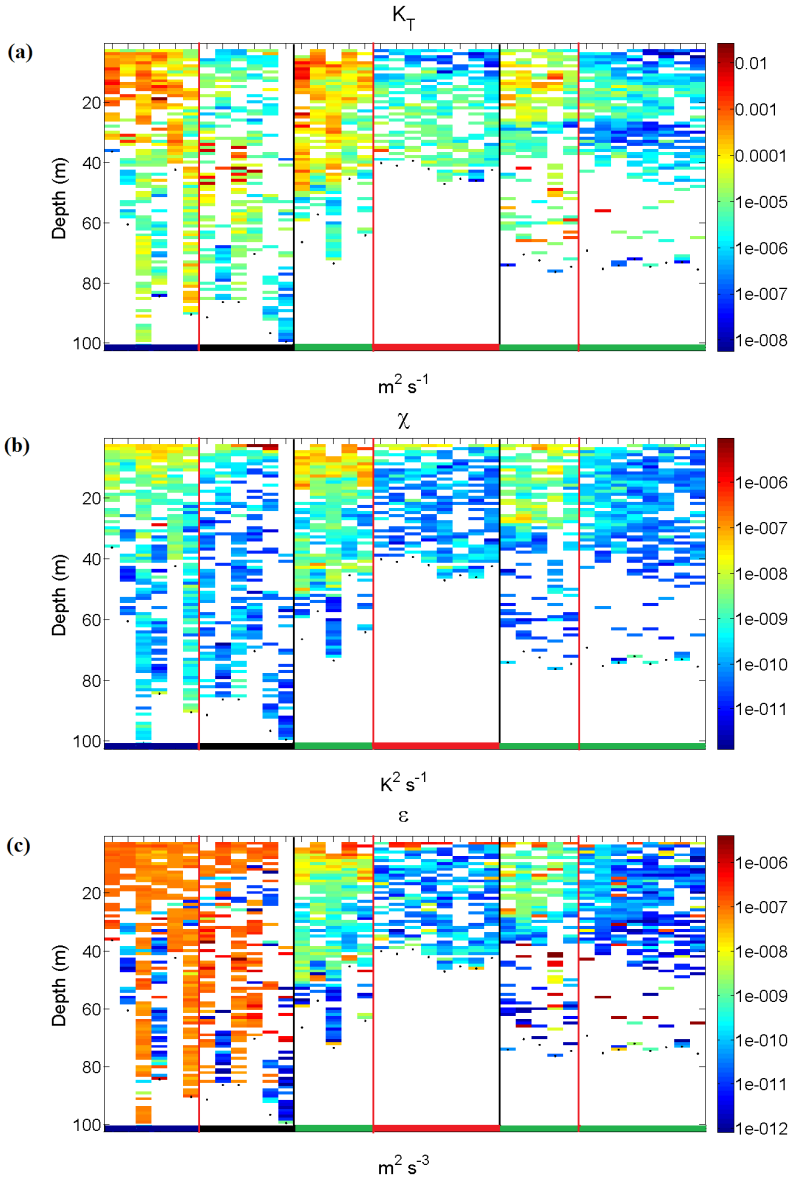

Figure 5: Depth binned turbulence characteristics (K_T, χ and ε) measured from 5-7 March. The vertical black lines indicate the difference between the days, the vertical red lines indicate the difference between morning and afternoon. The colors on the x axis indicates the station where the measurements were done similar as in Fig. 1. The small black dots represent the maximum depth of the measurement.

produced most reliable results. When there was no MLD found according to the criterion above, the whole profile was averaged. This is done with an exception of the twelfth profile where the SCAMP started measuring at a depth of 39 meters. Again, a distinction is made between measurements done in the morning (before 13:00) and afternoon (after 13:00) to take into account the effect of changing wind stress.

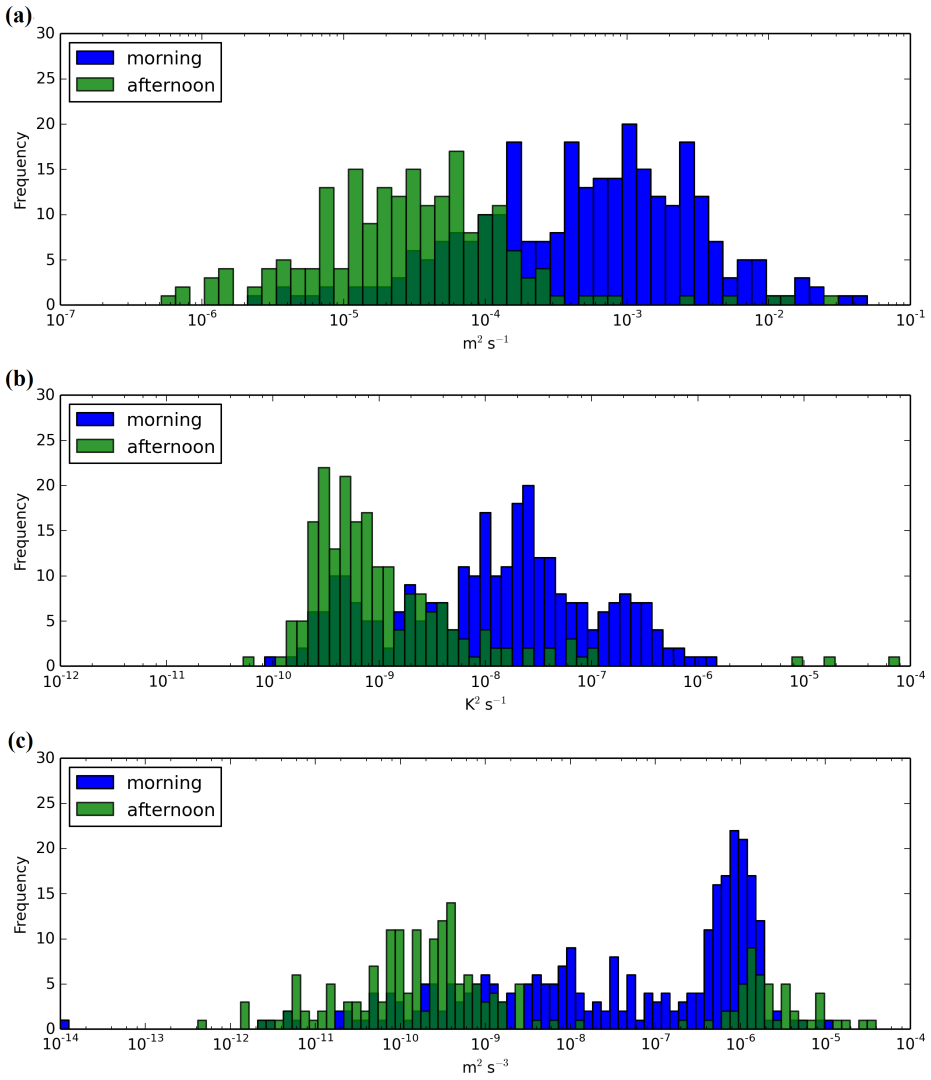

Figure 6: Diurnal variation of **(a)** K_T $(m^2 s^{-1})$, **(b)** χ $(K^2 s^{-1})$ and **(c)** ε $(m^2 s^{-3})$ in the ML. When morning values (blue) are plotted behind afternoon (green) values this is indicated by the dark green bars.

In Fig. 6 a-c a shift of the turbulence characteristics is seen where relatively high values of turbulence characteristics occur in the morning and reduced values in the afternoon. In the ML, the median of K_T in the morning is 5.93×10^{-4} m^2 s^{-1} and in the afternoon 3.11×10^{-5} m^2 s^{-1}. The median of χ in the morning is 1.49×10^{-8} K^2 s^{-1} and in the afternoon 6.86×10^{-10}

$K^2\ s^{-1}$. The median of ε in the morning is $9.16 \times 10^{-8}\ m^2\ s^{-3}$ and in the afternoon $3.29 \times 10^{-10}\ m^2\ s^{-3}$. The median was chosen because when using a logarithmic scale mean values are not representative. The relatively high values during the measurements done in the afternoon of March 5 can be seen as the rightmost green distribution in Fig. 6c.

According to the Osborn-Cox theory [19], a relationship between the vertical mixing coefficient K_T, the turbulent kinetic energy dissipation ε and the Brunt Väisälä frequency N^2 (s^{-2}) is expected to be

$$K_T = \Gamma \frac{\varepsilon}{N^2}, \tag{8}$$

where $\Gamma \approx 0.2$ is the so-called mixing efficiency. According to Ruddick et al. (1997) [23] this relation valid in turbulent circumstances (high Reynolds number). To investigate this relationship, a scatter plot is made between $\log(K_T)$ and $\log(\varepsilon/N^2)$ in Fig. 7a and between $\log(K_T)$ and $\log(N)$ in Fig. 7b.

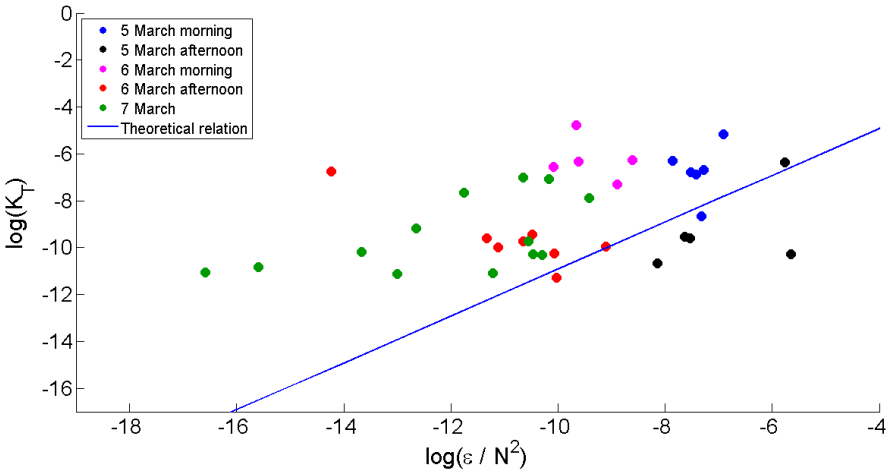

(a)

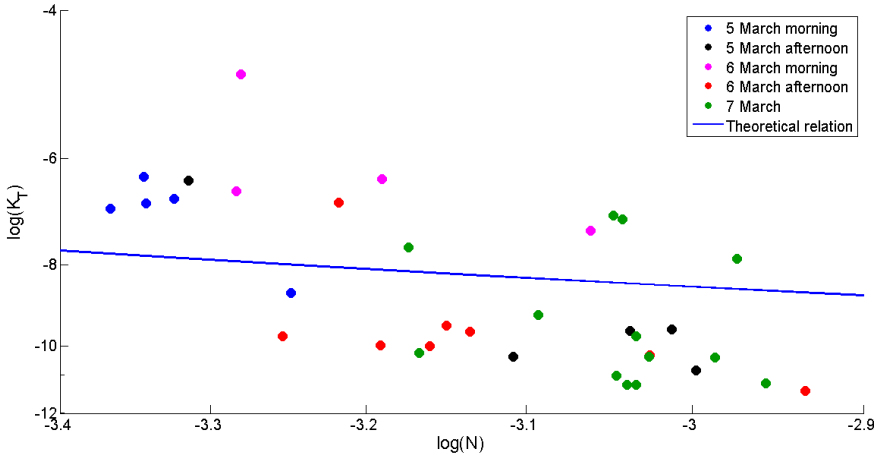

(b)

Figure 7: (a) Relation between $\log(K_T)$ and $\log(\varepsilon/N^2)$ (b) Relation between $\log(K_T)$ and $\log(N)$. The blue line in both figures is according to the Osborn-Cox theory.

Data plotted in Fig. 7a and b show strong variation around the theoretical blue line. According to theory, a linear relationship exists between $log(K_T)$ and $log(\frac{\varepsilon}{N^2})$ with a slope of 1 and intersection of the y-axis at y = $log(0.2)$. The data plotted in Fig. 7a shows a linear regression slope of 0.31 and Γ of 0.0041. When only the data measured in the morning, where the

circumstances are turbulent, is used to determine the mixing efficiency this equates to a slope of 0.26 and Γ of 0.011. Mixing efficiency is highly variable and cannot be described by a constant, values of mixing efficiency found are in the range of $\mathcal{O}$ $(10^{-}2)$ and $\mathcal{O}$ $(10^{-}3)$, one and two order of magnitudes smaller than the theoretical value.

3.3. Fluorescence and Chlorophyll-a

Calibration of the measured fluorescence data is done as described in Appendix B. Using this calibration, all the measured chl-a ($\mu g/L$) vertical profiles are shown in Fig. 8. In the upper layer of lake Garda sufficient light

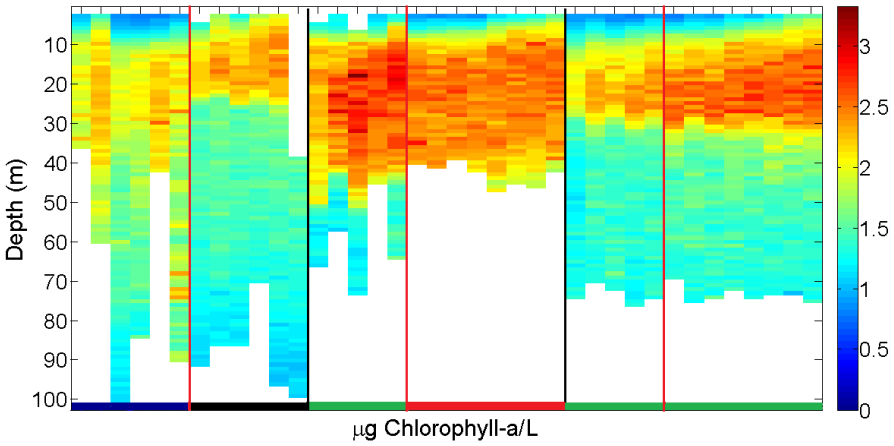

Figure 8: Chlorophyll-a profiles measured using the SCAMP fluorescence sensor on 5-7 March. Black lines indicate the difference between the days, red lines indicate the difference between morning and afternoon. The colors on the x-axis indicate the station where the measurements were done similar as in Fig. 1.

is present for phytoplankton to grow, the euphotic zone. Below the euphotic zone, because of turbidity of the water and shading by phytoplankton, a reduced amount of light is limiting phytoplankton growth. Highest concentration of chl-a are found in the middle of the ML, they reduce towards the surface and the bottom of the ML.

A clear ML is shown in the chl-a distribution with a strong gradient in the chl-a concentration at the MLD with an exception in the morning of March 5 where stratification was still weak and mixing to greater depths was possible.

During the lake Garda field trip surface chl-a concentrations were measured by MODIS AQUA. The penetration depth of the remote sensing measurements is dependent on the turbidity of the water column and remains difficult to determine. As an approximation we assume the penetration depth to be 10 meters. In Fig. 9 the average concentration of chl-a in the first 10 meters measured by the SCAMP is shown for the three different days. Measurements of MODIS AQUA are plotted at the corresponding time of the SCAMP measurement. A clear diurnal cycle is visible with relatively low

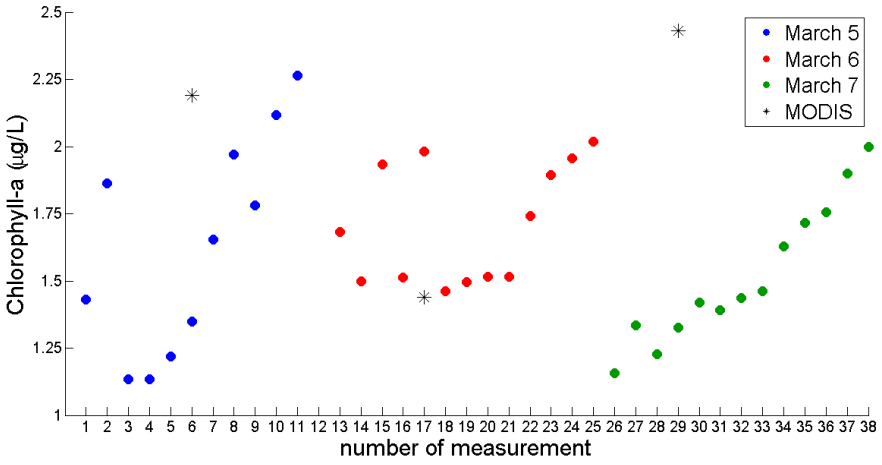

Figure 9: Chlorophyll-a concentration averaged over the first 10 meter of the water column measured by the SCAMP. For clarity, the data is divided into three different days. Black stars represent the chl-a measurements done by MODIS-AQUA.

concentrations in the morning and increasing concentrations during the day. In Fig. 8 it can be seen that the high chl-a concentrations in the middle of the ML spread towards the surface layer during the day. This can be related to the effect of waves on phytoplankton distribution. The effect of surface wind stress on vertical phytoplankton distribution is described by (Webster and Hutchinson et el. (1994) [28]). When the wind speed exceeds a critical value, phytoplankton is forced down into the water column. Observational evidence was found by Horne and Wrigly et al. (1975) [9], they found that wind speeds $>$ 2-3 $m\ s^{-1}$ were capable of mixing phytoplankton away from the water surface. Wind speeds of this magnitude are found at March 5-7 in the morning and at March 6 in the afternoon (Fig. 2).

MODIS AQUA measured values at March 5 and 7 are high compared to values measured with the SCAMP at the same time. At March 6 the chl-a concentration is too low compared to SCAMP measurement at the same time but is more on one line with surrounding measurements.

Figure 10 shows maps of chl-a retrieved concentrations measured by MODIS AQUA after applying BOMBER [7] during the lake Garda field trip.

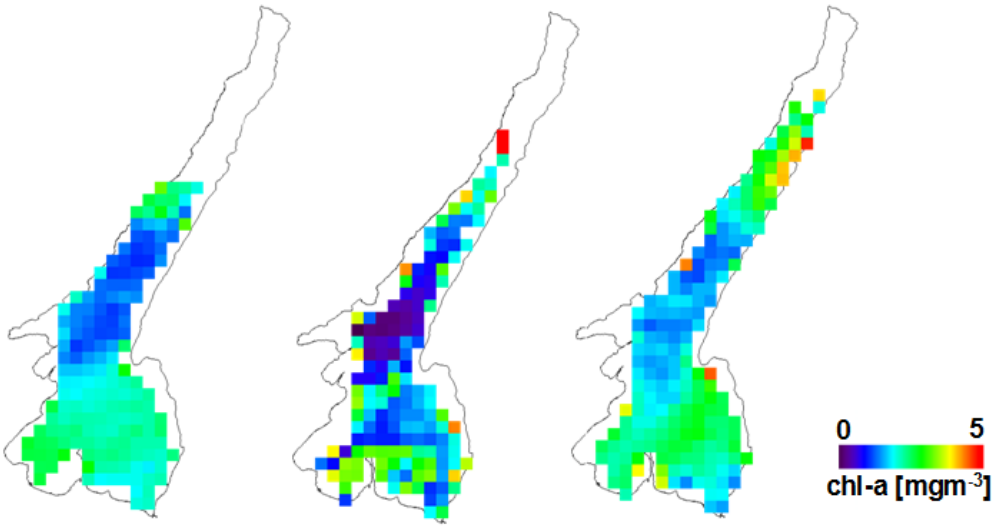

Figure 10: The MODIS AQUA-retrieved chl-a mg/L concentrations on March 5, 6 and 7, 2014.

Overall, chl-a concentrations show similar patterns and order of magnitude during days of the field trip. Measurements achieved on March 6 show more patchy patterns with respect to the day before and after, probably due to the high wind-speed during that day (Fig. 2). In the northern part where lake Garda is only 3-5 km wide the MODIS AQUA measurements are too coarse to produce data. Relative high chl-a concentrations are found in the southern and northern part. In the center concentrations are lower.

In Table 2, the measurements of chl-a based on filtrated water samples at different depths and surface measurements of MODIS AQUA are listed. Water samples are used to calibrate the fluorometer of the SCAMP. Assuming chl-a concentrations are constant in the surface layer surface water samples are compared with the mean value of the first 5 meters because the SCAMP

starts measuring at a depth of 2 meter. Satellite surface measurements are compared by taking the mean value of the first 10 meters of the SCAMP profile. The correlation between the water surface water samples, MODIS AQUA and SCAMP measurements at the same time is further discussed in Appendix A. Also listed are the nutrients $N\text{-}NO^{2-}$ + $N\text{-}NO^{3-}$ which are crucial nutrients for phytoplankton growth.

Date	**Station**	**Depth**	**Sample** chlor-a	**SCAMP** chlor-a	**MODIS** chlor-a	**SCAMP** chlor-a	**Sample** $N\text{-}NO^2/N\text{-}NO^3$
5-3	blue	surf	1.94	0.93	2.19	1.35	414.3
		45 m	2.43	2.55			422.8
5-3	black	surf	1.26	1.46	1.30		400.3
		30 m	1.34	1.38			411.2
6-3	green	surf	3.97	1.24	1.44	1.98	379.8
		45 m	1.40	1.42			419.2
6-3	red	surf	2.44	1.07	2.24		403.9
		45 m	2.04	2.31			437.4
7-3	green	15 m	2.60	0.96	2.43	1.33	390.2
		45 m	2.25	2.34			394.7

Table 2: Measurements of chl-a and nutrient concentrations ($\mu g/L$) during March 5-7 in lake Garda. Comparison of water samples and satellite measurements were done with SCAMP measurements at the same time and depth. Bolt measurement depths indicate measurements below the ML in the hypolimnion.

There are four measurements of chl-a and nutrients done below the ML in the hypolimnion. The concentrations of nutrients $N\text{-}NO^{2-}$ and $N\text{-}NO^{3-}$ are, as expected lower, in the ML where nutrients are assimilated by phytoplankton and stratification reduces the supply from below. Between mid autumn and begin summer nutrient concentrations in the ML are not the limiting factor for phytoplankton growth. On March 11 silica was measured in the Northern part of lake Garda (near Brenzone). It is an essential nutrient for the development of diatoms, and resulted to be above limiting concentration. Additional measurements of nutrients measured on March 11 are shown in Appendix D.

3.4. Connection between vertical mixing and chlorophyll-a

The correlation between K_T and the chl-a concentration is shown in Fig. 11. The plotted chl-a concentrations and K_T values are the averaged values in the ML (MLD defined same as in section 3.2).

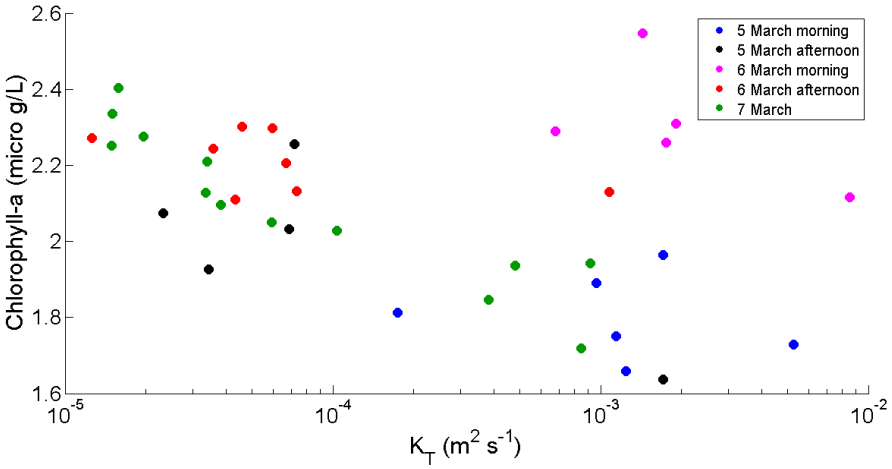

Figure 11: Correlation between K_T and chl-a in the ML. The colors of the plots represent the stations where the measurements were done.

A trend is visible in the data: the chl-a concentration decreases when the vertical mixing coefficient increases. March 5 and 7 show clear trends while March 6 shows high chl-a concentrations in the morning during high mixing.

Vertical mixing can limit the growth of phytoplankton because of 'critical turbulence'; if vertical mixing exceeds a critical value, phytoplankton is mixed out of the euphotic zone before it had the opportunity to grow and therefore growth may be reduced [18, 28]. Measurements done on March 11 in the northern part of lake Garda show that the depth of the euphotic zone is 22 m. At March 5 because of weak stratification phytoplankton is easily mixed to great depth below the euphotic zone.

High chl-a concentrations measured at March 6 in the morning could be related to "turbulence avoidance" by zooplankton. In normal circumstances zooplankton migrates to the surface at night to eat phytoplankton. In the excellent summary by Pringle (2007) [21] turbulence avoidance is described as the migration of zooplankton to deeper layer to avoid Ekman transport at the surface. Wind stress of 0.0398 to 0.1593 $N\ m^{-2}$ are described as sufficient to drive the turbulent sensitive species out of the Ekman circulation. Wind stress above this critical value are found at March 6 during the night (Fig. 3c).

4. Summary & Discussion

In this study we have presented in-situ and remote sensing data measured over three days in the beginning of March at the southern part of lake Garda. Measurements done at different stations, where differences in circumstances are small, are compared with each other. Data was obtained by the use of a free-fall microstructure profiler, water sampling and satellite measurements done by MODIS AQUA.

During the field trip a diurnal trend in the meteorological forcing was observed. Where relatively high wind speeds occurred in the morning and reduced wind speeds in the afternoon. Temperature profiles show a build up of stratification during the measuring period, the same signal is seen in measurements of fluorescence.

Measurements of K_T, χ and ε done in the ML show a diurnal cycle, high values of turbulence characteristics are found in the morning and reduced values in the afternoon. This variation can be related to the diurnal variation of wind stress induced mixing.

Surface chl-a concentration provided by MODIS AQUA show similar pattern during the field trip. With relative high concentration in the southern and northern part. Comparison between satellite and SCAMP measurements remain difficult because of variable maximum penetration depth of MODIS AQUA.

The correlation between the vertical mixing coefficient and the chl-a concentration measured in the ML show a clear trend, this indicates that wind stress induced mixing is limiting the phytoplankton growth.

Temperature profiles measured at March 5 show homogeneous temperature profiles where phytoplankton is mixed down to a great depth, indicating that critical turbulence is limiting phytoplankton growth. Other temperature profiles show a more stratified profile which reduces the effect of critical turbulence on chl-a concentrations.

Measurements of high chl-a concentration done at March 6 in the morning can be related to absence of zooplankton in the night before because of "turbulence avoidance" [21]. Where zooplankton stays in the deeper parts of the water column to avoid wind driven Ekman transport. Proof of the absence of zooplankton could not be provided because zooplankton concentrations were not measured.

Chl-a surface concentrations increase during the day, this can be related to wind induced waves which force the phytoplankton down into the water

column [28]. This is also seen in the chl-a concentrations measured in the first 10 meters of the water column. When there are relatively high wind speeds the concentration near the surface is relatively low while during reduced wind speeds the chl-a concentration increases.

The determination of the mixing efficiency on the basis of the Osborn & Cox relation [19] remain difficult because of the short measurement period and highly variable turbulence characteristics.

Measurements done in the southern part of lake Garda were done to gather more knowledge about the effects of vertical mixing on phytoplankton concentration/distribution. These appeared to be the first of turbulence characteristics in lake Garda. High resolution measurements of fluorescence distribution show interesting diurnal variation which can be related to different external factors. These results can be used for validation of satellite chl-a measurements in the upper layer of lake Garda. Hopefully our results will stimulate further investigation in this field.

5. References

[1] W. Bleiker and F. Schanz. Influence of environmental factors on the phytoplankton spring bloom in lake zürich. *Aquatic Sciences*, 51(1):47–58, 1989.

[2] M. Bresciani, R. Bolpagni, F. Braga, A. Oggioni, and C. Giardino. Retrospective assessment of macrophytic communities in southern lake garda (italy) from in situ and mivis (multispectral infrared and visible imaging spectrometer) data. *Journal of Limnology*, 71(1):e19, 2012.

[3] T. M. Dillon and D. R. Caldwell. The batchelor spectrum and dissipation in the upper ocean. *Journal of Geophysical Research: Oceans (1978–2012)*, 85(C4):1910–1916, 1980.

[4] F. M. Fozdar, G. J. Parkar, and J. Imberger. Matching temperature and conductivity sensor response characteristics. *Journal of Physical Oceanography*, 15(11):1557–1569, 1985.

[5] C. Giardino, V. E. Brando, A. G. Dekker, N. Strömbeck, and G. Candiani. Assessment of water quality in lake garda (italy) using hyperion. *Remote Sensing of Environment*, 109(2):183–195, 2007.

[6] C. Giardino, G. Candiani, M. Bresciani, M. Bartoli, and L. Pellegrini. Multi-spectral ir and visible imaging spectrometer (mivis) data to assess optical properties in shallow waters.

[7] C. Giardino, G. Candiani, M. Bresciani, Z. Lee, S. Gagliano, and M. Pepe. Bomber: A tool for estimating water quality and bottom properties from remote sensing images. *Computers & Geosciences*, 45:313–318, 2012.

[8] B. Holben, T. Eck, I. Slutsker, D. Tanre, J. Buis, A. Setzer, E. Vermote, J. Reagan, Y. Kaufman, T. Nakajima, et al. Aeroneta federated instrument network and data archive for aerosol characterization. *Remote sensing of environment*, 66(1):1–16, 1998.

[9] A. Horne and R. Wrigley. The use of remote sensing to detect how wind influences planktonic blue-green algal distribution. *Verhandlungen Internationale Vereinigung Limnologie*, 19:784–971, 1975.

[10] E. Jurado, H. van der Woerd, and H. Dijkstra. Microstructure measurements along a quasi-meridional transect in the northeastern atlantic ocean. *Journal of Geophysical Research*, 117(C4):C04016, 2012.

[11] S. Y. Kotchenova, E. F. Vermote, R. Matarrese, F. J. Klemm Jr, et al. Validation of a vector version of the 6s radiative transfer code for atmospheric correction of satellite data. part i: Path radiance. *Applied optics*, 45(26):6762–6774, 2006.

[12] Z. Lee, K. L. Carder, C. D. Mobley, R. G. Steward, and J. S. Patch. Hyperspectral remote sensing for shallow waters. i. a semianalytical model. *Applied Optics*, 37(27):6329–6338, 1998.

[13] Z. Lee, K. L. Carder, C. D. Mobley, R. G. Steward, and J. S. Patch. Hyperspectral remote sensing for shallow waters. 2. deriving bottom depths and water properties by optimization. *Applied Optics*, 38(18):3831–3843, 1999.

[14] S. Levitus, J. I. Antonov, T. P. Boyer, and C. Stephens. Warming of the world ocean. *Science*, 287(5461):2225–2229, 2000.

[15] C. J. Lorenzen. Vertical distribution of chlorophyll and phaeo-pigments: Baja california. In *Deep Sea Research and Oceanographic Abstracts*, volume 14, pages 735–745. Elsevier, 1967.

[16] D. A. Luketina and J. Imberger. Determining turbulent kinetic energy dissipation from batchelor curve fitting. *Journal of atmospheric and oceanic technology*, 18(1):100–113, 2001.

[17] N. Oakey. Determination of the rate of dissipation of turbulent energy from simultaneous temperature and velocity shear microstructure measurements. *Journal of Physical Oceanography*, 12(3):256–271, 1982.

[18] A. Omta, S. Kooijman, and H. Dijkstra. Critical turbulence revisited: The impact of submesoscale vertical mixing on plankton patchiness. *Journal of Marine Research*, 66(1):61–85, 2008.

[19] T. R. Osborn and C. S. Cox. Oceanic fine structure. *Geophysical & Astrophysical Fluid Dynamics*, 3(1):321–345, 1972.

[20] F. Peeters, D. Straile, A. Lorke, and D. Ollinger. Turbulent mixing and phytoplankton spring bloom development in a deep lake. *Limnology and Oceanography*, 52(1):286–298, 2007.

[21] J. M. Pringle. Turbulence avoidance and the wind-driven transport of plankton in the surface ekman layer. *Continental Shelf Research*, 27(5):670–678, 2007.

[22] B. Ruddick, A. Anis, and K. Thompson. Maximum likelihood spectral fitting: The batchelor spectrum. *Journal of Atmospheric and Oceanic Technology*, 17(11):1541–1555, 2000.

[23] B. Ruddick, D. Walsh, and N. Oakey. Variations in apparent mixing efficiency in the north atlantic central water. *Journal of Physical Oceanography*, 27(12):2589–2605, 1997.

[24] N. Salmaso. Effects of climatic fluctuations and vertical mixing on the interannual trophic variability of lake garda, italy. *Limnology and Oceanography*, 50(2):553–565, 2005.

[25] M. Scheffer, D. Straile, E. H. van Nes, and H. Hosper. Climatic warming causes regime shifts in lake food webs. *Limnology and Oceanography*, 46(7):1780–1783, 2001.

[26] U. Sommer. *Plankton Ecology, succession in plankton communities.* Springer, 1989.

[27] G. I. Taylor. The spectrum of turbulence. *Proceedings of the Royal Society of London. Series A-Mathematical and Physical Sciences*, 164(919):476–490, 1938.

[28] I. T. Webster and P. A. Hutchinson. Effect of wind on the distribution of phytoplankton cells in lakes revisited. *Limnology and Oceanography*, 39(2):365–373, 1994.

Appendix A: Calibration of SCAMP fluorometer data

The SCAMP measures fluorescence in voltages and is supplied uncalibrated by PME. Calibration is done by taking water samples at several depths using a Van Dorne bottle. During the Lake Garda field trip 5 samples are taken at the surface and 6 at a greater depth (table 2). The samples taken at the surface are not used for calibration because the SCAMP starts measuring at a depth of 2 meters. Because the uncertainty of the depth of the water samples, the two surrounding measured fluorescence segments are also taken into account. Out of these three values per water sample the values are chosen which are on one line. This method is an approximation to the real values and has a large uncertainty. Without the calibration the measurements of fluorescence still provide a qualitative indication of the distribution of chl-a in the water column.

In Fig. 12 measured chl-a concentrations by the SCAMP and water samples are plotted. The sample taken on March 6 at a depth of 45 meters in the afternoon was not used because SCAMP measurements at this station were not all deep enough.

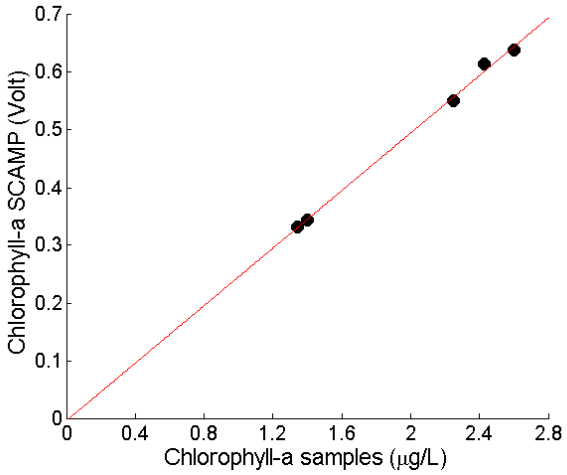

Figure 12: Correlation between chl-a measurements done by the SCAMP (volt) and water samples ($\mu g/L$).

The conversion factor to convert the SCAMP measurements from voltage to $\mu g/L$ out of figure 12 is 4.148.

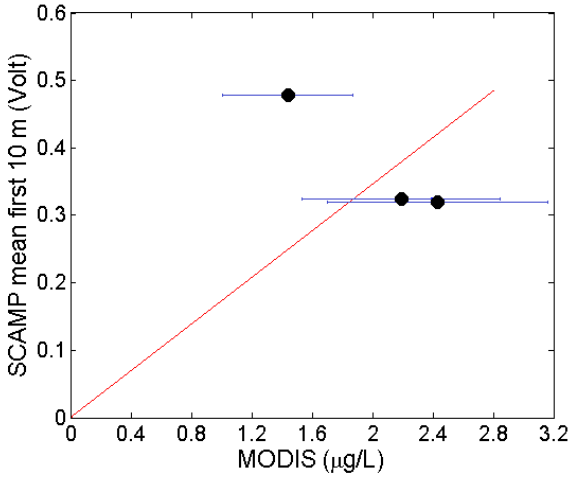

Figure 13: Correlation between chl-a measurements by MODIS AQUA ($\mu g/L$) and the SCAMP (volt). For the SCAMP measurements the first 10 meters are averaged.

The surface chl-a satellite measurements done by MODIS AQUA can also be used for calibration of the SCAMP fluorometer. Measurements of MODIS AQUA were done at 12:10, 12:50 and 11:55 UTC. The depth of the satellite measurements depends on the turbidity of the water and is different for every profile because of phytoplankton growth and distribution. The assumption is made that the satellite measures until a depth of 10 meters. The first 10 meters of the SCAMP profile are averaged and compared with the satellite measurements in figure 13.

Because of the influence of turbidity on the satellite measurements it is difficult to determine the maximum penetration depth of MODIS AQUA. Because of the distribution and number of the points shown in Fig. 13 it is chosen to not use the satellite measurements as calibration for the SCAMP fluorometer. The conversion factor determined by the in-situ measurements is used for calibration.

Appendix B: Maximum likelihood Batchelor spectrum fitting

The Batchelor wave number k_B can estimated by fitting the observed temperature spectrum to a theoretical Batchelor spectrum. The observed vertical temperature profile is divided in segments of 1 meter. By means of

fast Fourier transform using a hamming window a spectrum of every segment is made. The observed spectrum is fitted to the theoretical Batchelor spectrum (equation 9).

$$S_{th}(k) = S_B(k) + S_n(k) \tag{9}$$

The theoretical spectrum is built up out of the analytic expression for the Batchelor spectrum S_B (equation 10) and the instrumental noise spectrum S_n. The magnitude of the noise is different for every SCAMP and can be set within the MATLAB routine.

$$S_B(k; k_B, \chi) = (q/2)^{\frac{1}{2}} \chi k_B^{-1} \kappa_T^{-1} f(\alpha) \tag{10}$$

The non dimensional shape of the spectrum is given by $f(\alpha)$ (equation 11) where α is the non-dimensional wave number (equation 12) and k is the wave number (radians/unit length). q is a universal constant range between 3.4-4.1 which is set as 3.4 to match the value used in the SCAMP software [16].

$$f(\alpha) = \alpha \left(e^{-\alpha^2/2} - \alpha \int_{\alpha}^{\infty} e^{-x^2/2} dx \right) \tag{11}$$

$$\alpha = k k_B^{-1} \sqrt{2q} \tag{12}$$

In this research we made use of the maximum likelihood estimate (MLE) (equation 13) to find the best fit between the observed and theoretical spectrum. This technique has an explicit incorporation of the instrumental noise. This offered significant improvement over least square techniques which is normally used. The best fit between the theoretical and observed spectrum is found by maximizing C11.

$$C11 = \sum_{i=1}^{N} ln \left\{ \frac{d}{S_B(k_i; k_B, \chi_\theta) + S_n(k_i)} * \chi_d^2 \left[\frac{dS_{obs}(k_i)}{S_B(k_i; k_B, \chi_\theta) + S_n(k_i)} \right] \right\}, \tag{13}$$

where d is the number of degrees of freedom. An example of a fit between the spectra is given in figure 14. The power spectral density $((\frac{^\circ C}{m})^2/\frac{cyc}{m})$ is plotted against the wave number (cyc/m).

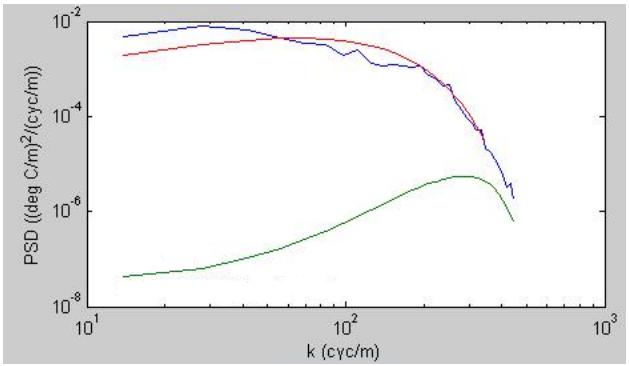

Figure 14: Example of a fit between theoretical and observed spectra. The red line represents the theoretical Batchelor spectrum the blue line the observed spectrum and the green line the modeled noise.

Some observed temperature gradient spectra can be difficult to fit. When the wave number is higher instrumental noise becomes more important and can have an influence on the fit between the spectra. When the amplitude of the noise is too high comparing the observations this gives a problem while fitting the theoretical Batchelor shape at the high wave number end. An other problem can be internal wave and fine-structure contamination at the low wave number end of the spectra. Because the wave numbers are to high to fit a theoretical Batchelor spectrum. These limiting Batchelor wave numbers, which can be used to fit the observations, rely on the range which can be measured. k_L is the lowest wave number at which the S_{obs} and S_{th} intersect and k_n is the noisy wave number which depends on the noise of the SCAMP [16].

To determine if a fit between the observed values and the Batchelor spectrum is sufficiently good. There are three criteria that the fit should satisfy.

1. Signal-noise ratio; if the integrated signal-noise ratio is smaller than 1.3 the segment is rejected because the level of noise is too high comparing the signal.
2. The likelihood ratio; in this rejection criteria the Batchelor spectrum fit (which had a sharp cutoff (fits well for a certain Batchelor wave number)) is compared with the power law (equation 14) which doesn't have a cutoff.

$$S_{th} = Ak^{-b} + S_n \tag{14}$$

If the Batchelor fit does not provide a significantly better fit than the powerlaw fit then that segment is rejected because it doesn't have a clear cutoff. The two spectral fits are compared by equation 15. If L_{ratio} is smaller than 2 the segment is rejected. This value is set as 2 out of experience [22].

$$L_{ratio} = log_{10}\left(\frac{Batchelor fit}{Powerlaw fit}\right) \tag{15}$$

3. Variance over the fit; if the variance over the fit is too large the segment is rejected. The mean absolute deviation is calculated using equation

$$MAD = \frac{1}{n}\sum_{k_i=k_1}^{k_n}\left|\frac{S_{obs}}{S_{th}} - \left\langle\frac{S_{obs}}{S_{th}}\right\rangle\right| \tag{16}$$

The value of variance for which a segment is rejected depend on the degrees of freedom. A segment is rejected when

$$MAD \quad < \quad 2 * \sqrt{2 * d} \tag{17}$$

When d is higher more variance around the Batchelor fit is allowed.

Figure 15 is an example of a bad fit where the theoretical Batchelor spectrum is fitted to the noise. This is a example of a segment that is rejected by the rejection criteria listed above.

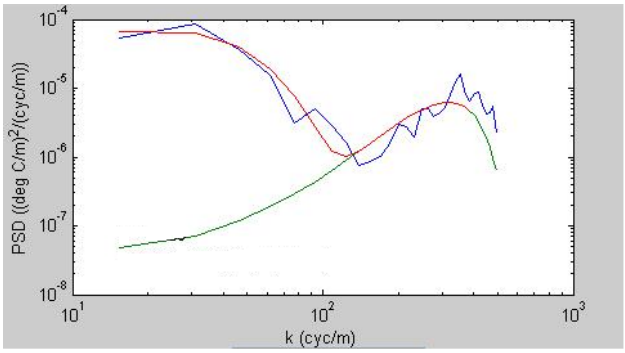

Figure 15: Example of a bad-fit between theoretical and observed spectra. The red line represents the theoretical Batchelor spectrum the blue line the observed spectrum and the green line the modeled noise.

Batchelor curve fitting can only be used when the Taylor hypothesis of frozen "frozen turbulence" is valid [27]. The = hypothesis is generally considered to be valid if variations in the fluctuating velocities are small compared with the velocity of the SCAMP. The speed of the SCAMP is ideally reasonably greater than the largest turbulent velocity fluctuations. When the SCAMP velocity is to high roll-off becomes a problem. The turbulence velocity scales as $u \sim (\varepsilon * L)^{\frac{1}{3}}$. In an energetic environment ε is around 10^{-5} and L is around 0.1. This given a u of 0.01 $m\ s^{-1}$ thus 0.1 $m\ s^{-1}$ is a good compromise between sensor roll-off and the Taylor hypothesis [16].

Appendix C: MODIS-aqua corrections

MODIS AQUA (MYD021KM product) Level 1B data were used to assess chl-a concentrations. Radiance products were corrected for the atmospheric effect with the 6SV1 code (Second Simulation of a Satellite Signal in the Solar Spectrum, Vector, version 1) [11]. The code was run with an aerosol model typical for the Po plan valley; the atmospheric profiles were set according to the latitude and the season (i.e. Midlatitude winter). For each image, the aerosol optical thickness at the time of MODIS overpass was derived from AERONET [8] by interpolating data gathered from the stations closest to Lake Garda (i.e., Ispra, Venice and Modena). The spectral inversion procedure BOMBER [7], implementing a four-component bio-optical model [12],[13], was used to estimate chl-a from MODIS-derived Rrs data. The bio-optical model parameterisation relies on a comprehensive dataset of concentrations and optical properties we measured in Lake Garda in recent years [2],[6]. Such parameterisation has been further updated by integrating data sampled during the three days campaign presented in this study.

Appendix D: Additional nutrient measurements

Table 3 shows measurements done in the Northern part of lake Garda near Brenzone four days after the lake Garda field trip.

Depth	N-NO3 ($\mu g/L$)	N-NH3 ($\mu g/L$)	SiO2 (mg/L)
0	337,24	5	1,14
10	331,41	5	1,15
20	341,49	5	1,20
60	350,10	5	1,20
100	367,40	5	1,49

Table 3: Measurements of nutrients done at the Northern part of lake Garda (near Brenzone) at March 11.

Measurements of nutrients are as expected lower than during the lake Garda field trip because of the increasing depth of lake Garda towards the North. Nutrient concentrations measured are not limiting phytoplankton growth.

Acknowledgments

Special thanks to Fiona R. vd Burgt and Erwin Lambert for discussing previous versions of the article. Without there help this article would not be of the same quality. We also greatly acknowledge all the members of the student room (2014), in special Leon Saris, Sharon van Geffen, Lotte de Vos and Sjoerd Janson, for mental support and the organization of coffee-breaks and outdoor activities when needed. Thanks Henk and Lisa for support, interesting meetings and the great time we had at lake Garda. Most of all thanks goes out to the support I got from my mother José and two brothers Aart-Jan & Jelmer.